JIPB Journal of Integrative Plant Biology

Research Article
https://doi.org/10.1111/jipb.13151

Increasing yield potential through manipulating of an *ARE1* ortholog related to nitrogen use efficiency in wheat by CRISPR/Cas9[oo]

Jiahui Zhang[1], Huating Zhang[1,2], Shaoya Li[1], Jingying Li[1], Lei Yan[1] and Lanqin Xia[1]*

1. Institute of Crop Sciences, Chinese Academy of Agricultural Sciences, Beijing 100081, China
2. School of Agricultural Sciences, Zhengzhou University, Zhengzhou 450001, China

*Correspondence: Lanqin Xia (E-mail: xialanqin@caas.cn)

Jiahui Zhang

Lanqin Xia

ABSTRACT

Wheat (*Triticum aestivum* L.) is a staple food crop consumed by more than 30% of world population. Nitrogen (N) fertilizer has been applied broadly in agriculture practice to improve wheat yield to meet the growing demands for food production. However, undue N fertilizer application and the low N use efficiency (NUE) of modern wheat varieties are aggravating environmental pollution and ecological deterioration. Under nitrogen-limiting conditions, the rice (*Oryza sativa*) *abnormal cytokinin response1 repressor1* (*are1*) mutant exhibits increased NUE, delayed senescence and consequently, increased grain yield. However, the function of *ARE1* ortholog in wheat remains unknown. Here, we isolated and characterized three *TaARE1* homoeologs from the elite Chinese winter wheat cultivar ZhengMai 7698. We then used CRISPR/Cas9-mediated targeted mutagenesis to generate a series of transgene-free mutant lines either with partial or triple-null *taare1* alleles. All transgene-free mutant lines showed enhanced tolerance to N starvation, and showed delayed senescence and increased grain yield in field conditions. In particular, the *AABBdd* and *aabbDD* mutant lines exhibited delayed senescence and significantly increased grain yield without growth defects compared to the wild-type control. Together, our results underscore the potential to manipulate *ARE1* orthologs through gene editing for breeding of high-yield wheat as well as other cereal crops with improved NUE.

Zhang, J., Zhang, H., Li, S., Li, J., Yan, L., and Xia, L. (2021). Increasing yield potential through manipulating of an *ARE1* ortholog related to nitrogen use efficiency in wheat by CRISPR/Cas9. J. Integr. Plant Biol. **63:** 1649–1663.

INTRODUCTION

Bread wheat (*Triticum aestivum* L., 2n = 42, AABBDD) is a staple food crop consumed by more than 30% of the world's population. Nitrogen (N) fertilizer is applied broadly in agriculture to improve wheat yield to meet the growing demands for food production. However, the widely cultivated semi-dwarf 'Green Revolution' wheat varieties with increased yield potential resulted in contingent effects of reduced N-use efficiency (NUE), in fact, most modern wheat varieties only absorb less than 40% of the supplied N (Li et al., 2018). The remaining N is released to the environment through leaching and volatilization (Good and Beatty, 2011). In consequence, the low NUE of wheat and undue N fertilizer applications are aggravating environmental pollution and ecological deterioration (Li et al., 2021a). Improving NUE will therefore improve the sustainability of wheat production.

Ongoing studies have made some impressive progress in understanding and increasing NUE in crop plants (Hu et al., 2015; Li et al., 2018; Wang et al., 2018a; Wang et al., 2018b; Gao et al., 2019; Tang et al., 2019; Xu et al., 2019; Wang et al., 2021; Zhang et al., 2021). NUE depends on multiple physiological processes including N uptake, assimilation, metabolism, allocation, and remobilization. Plants take up nitrate (NO_3^-) and ammonium (NH_4^+) via the plasma membrane-localized nitrate transporters (NRTs) and ammonium transporters (AMTs) (Miller et al., 2007; Xu et al., 2012). Nitrate is converted to ammonium by nitrate reductase (NR) and nitrite reductase (NiR). Then, ammonium is assimilated into amino acids via the glutamine synthetase (GS) and glutamine 2-oxoglutarate amidotransferase (GOGAT) (Yang et al., 2016; Lv et al., 2021). Ferredoxin-dependent glutamate 2-oxoglutarate aminotransferase (Fd-GOGAT) and nicotinamide adenine dinucleotide-dependent glutamate 2-oxoglutarate aminotransferase (NADH-GOGAT) are two different forms of GOGAT that use ferredoxin and NADH as the electron donors, respectively. Fd-GOGAT is primarily located in leaf chloroplasts, whereas NADH-GOGAT is predominantly localized in non-photosynthetic plastids (Temple et al., 1998; Forde and Lea, 2007). During N remobilization, *Fd-GOGAT* plays an important role in ammonium reassimilation in photosynthetic tissues and *NADH-GOGAT* assimilates ammonium in non-photosynthetic cells (Lea and Miflin, 2003; Quraishi et al., 2011).

Genetic studies in rice have identified additional factors involved in NUE. The *abnormal cytokinin response1 repressor1* (*are1*) mutant was identified as a suppressor of a rice *fd-gogat* mutant defective in N assimilation. Loss-of-function mutations in rice *ARE1* result in delayed senescence, enhanced NUE and increased grain yield under N-limiting condition (Wang et al., 2018b). The rice transcription factor *Grain number*, *plant height*, *and heading date 7* (*Ghd7*) directly represses the expression of *ARE1* to positively regulate NUE and grain yield. The *Ghd7-ARE1* regulatory module has undergone diversifying selection. Combining of the elite alleles of *Ghd7* and *ARE1* significantly improves NUE and grain yield under low N conditions (Wang et al., 2021). These results indicate that *ARE1* orthologs play important roles in NUE and might be a good candidate to improve NUE in wheat and other major cereal crops. However, the *ARE1* ortholog in wheat has not been functionally characterized.

Although the clustered regularly interspaced short palindromic repeats (CRISPR)/CRISPR-associated protein 9 (Cas9) has been extensively applied for functional genomics studies and crop improvement (Ma et al., 2015; Li et al., 2019; Biswas et al., 2020; Liu et al., 2020; Zhan et al., 2021), generating targeted mutations in common wheat remains challenging due to its complex hexaploid genome. So far, only a few agronomically important traits in wheat have been successfully improved through CRISPR/Cas9 such as grain size and weight (Zhang et al., 2018; Wang et al., 2018c; Wang et al., 2019; Zhang et al., 2019), decreased gliadin content (Sánchez-León et al., 2018), increased resistant starch (Li et al., 2021b), increased powdery mildew resistance (Wang et al., 2014), and improved tolerance to pre-harvest sprouting (Abe et al., 2019). CRISPR/Cas9 has also been used in haploid induction (Liu et al., 2020; Lv et al., 2020), male sterility (Okada et al., 2019), and multiplex gene editing (Luo et al., 2021) in wheat. To date, increasing wheat NUE through manipulating key genes involved in N uptake and assimilation by genome editing has not been documented.

In the context of global climate change, increasing population, and diminishing farmland, it is essential to resilient wheat production by improving NUE, decreasing the N application, and maintaining the yield stability. Here, we isolated and functionally characterized a rice *ARE1* ortholog in the elite Chinese wheat variety cultivar ZhengMai 7698 (ZM). We analyzed the subcellular localization and spatial expression patterns of the three homoeologs in wheat. We then generated a series of transgene-free mutant wheat lines through CRISPR/Cas9-mediated targeted mutagenesis of *TaARE1*. We observed the development of roots in different mutant lines in response to N starvation and supply at different concentrations under hydroponic conditions. Among these mutant lines, the *AABBdd* and *aabbDD* mutant lines, rather than the *aabbdd* triple-null mutant line, exhibited significantly enhanced NUE, delayed senescence, and increased grain yield without growth penalty compared to the wild-type control in field conditions. Thus, we successfully generated novel wheat germplasm with enhanced NUE and improved grain yield. Our results demonstrated that harnessing *ARE1* orthologs through gene editing could be an alternative way to improve NUE and thus enhance grain yield of wheat and other major cereal crops.

RESULTS

Cloning and characterization of *TaARE1*

We identified a *TaARE1* ortholog in the elite Chinese winter wheat cultivar ZM using the amino acid and nucleotide sequences of *OsARE1* (*LOC _Os08g12780*) to conduct BLAST searches against the databases of the International Wheat Genome Sequencing Consortium, EnsemblPlants (http://plants.ensembl.org/), and a BAC library of the elite Chinese wheat variety AiKang 58 (AK). The three homoeologs *TaARE1* genes are located on chromosomes 7AS (*TaARE1-A*, A subgenome short arm), 7BL (*TaARE1-B*, B subgenome long arm), and 7DS (*TaARE1-D*, D subgenome short arm). We also isolated their full-length cDNA sequences. The genomic sequences of the three *TaARE1* homoeologs consisted of seven exons and six introns (Figure 1A). The cDNA sequences of the three *TaARE1* homoeologs were all 1266 bp in length, sharing a common conserved domain. Only 19 single-nucleotide polymorphism (SNPs) differences exist among the three homoeologs (Figure S1). We constructed a phylogenetic tree based on the full-length

predicted amino acid sequences of three TaARE1 homoeologs and other plants, and the phylogenetic analysis showed that TaARE1-A, TaARE1-B, and TaARE1-D are closely related to HvARE1 in barley (*Hordeum vulgare*) (Figure 1B). To examine the subcellular localization of the TaARE1 proteins, we transiently expressed a fusion of TaARE1-A to yellow fluorescent protein (YFP). When transiently expressed in wheat protoplasts, TaARE1-A-YFP localized in chloroplasts, indicating that TaARE1-A is a chloroplast-localized protein (Figure 1C). To analyze the expression profile of the three *TaARE1* homoeologs, we designed specific primers for *TaARE1-A*, *TaARE1-B*, and *TaARE1-D* and used reverse transcription quantitative PCR (RT-qPCR) to measure their transcript levels in different tissues at the grain-filling stage. The result showed that *TaARE1-A* had relatively higher expression level compared with *TaARE1-B* and *TaARE1-D* (Figure 1D). In addition, the three *TaARE1* homoeologs were expressed in all tissues; however, relatively higher expression levels of *TaARE1-B* and *TaARE1-D* were detected in roots and grains at the grain-filling stage, respectively (Figure 1D).

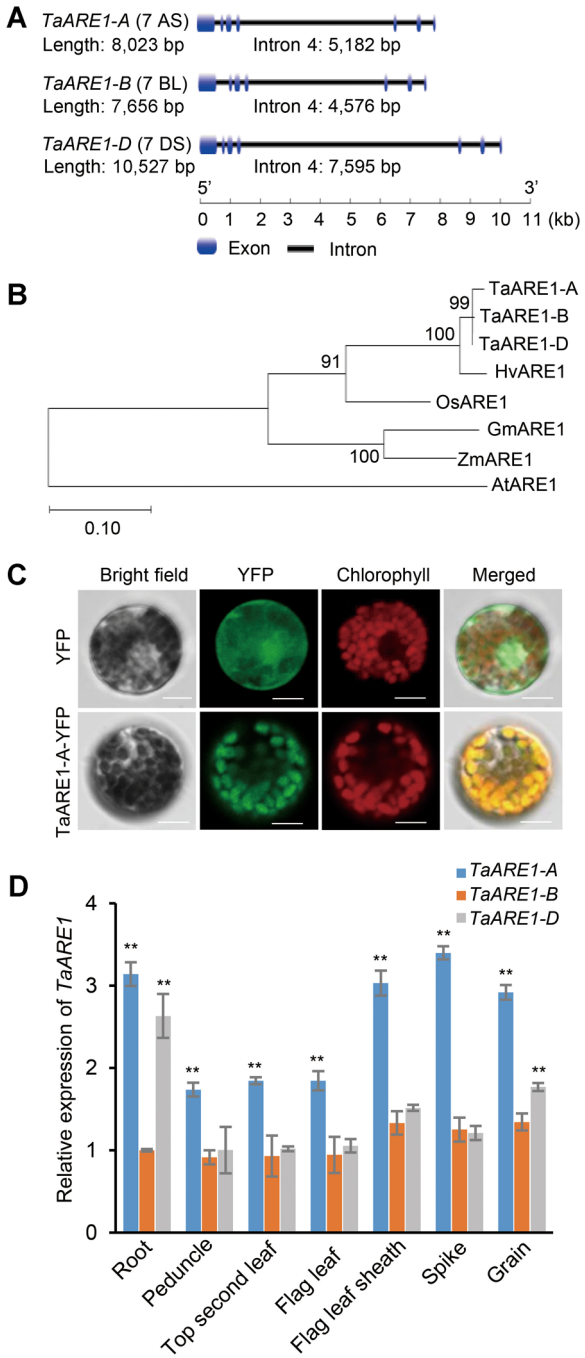

CRISPR/Cas9-mediated targeted mutagenesis of *TaARE1* in wheat

To examine the function of the TaARE1 homoeologs, we used CRISPR/Cas9 to generate loss-of-function mutants. To this end, we designed two gRNAs targeting the conserved sequences in the first and the fourth exon of the *TaARE1-A*, *TaARE1-B*, and *TaARE1-D* (Figure 2A). The gRNA2 contained a *Bts* CI restriction site that was used for screening mutants through a polymerase chain reaction-based restriction enzyme (PCR/RE) digestion assay (Figure 2A). The gRNA1 and gRNA2 cassettes driven by the *TaU6* promoter were cloned into the vector pCXUN-Ubi-Cas9-Nos-35S-hptII-Nos either alone or simultaneously (Figure 2B). Then, these three CRISPR/Cas9 vectors were separately transformed into immature

Figure 1. Characterization of *TaARE1*

(**A**) Gene structure of *TaARE1-A, TaARE1-B*, and *TaARE1-D*. Exons and introns are shown as blue boxes and black line, respectively. The full-length genomic sequence of *TaARE1-A* is 8,023 bp, containing seven exons (exon 1: 588 bp, exon 2: 86 bp, exon 3: 174 bp, exon 4: 115 bp, exon 5: 98 bp, exon 6: 136 bp, exon 7: 69 bp) and six introns (intron 1: 206 bp, intron 2: 98 bp, intron 3:169 bp, intron 4: 5182 bp, intron 5: 680 bp, intron 6: 422 bp). The full-length genomic sequence of *TaARE1-B* is 7656 bp, containing seven exons (the length of each exon is same as *TaARE1-A*) and six introns (intron 1: 444 bp, intron 2: 98 bp, intron 3:169 bp, intron 4: 4,576 bp, intron 5: 683 bp, intron 6: 420 bp). The full-length genomic sequence of *TaARE1-D* is 10,527 bp, containing seven exons (the length of each exon is same as *TaARE1-A*) and six introns (intron 1: 191 bp, intron 2: 98 bp, intron 3:166 bp, intron 4: 7,595 bp, intron 5: 677 bp, intron 6: 534 bp). (**B**) Phylogenetic tree of ARE1 and its homoeologs in plants. GenBank accession number and transcript assembly number for each sequence used in the tree are listed below: TaARE1-A (TraesCS7A02G286400, KAF7095826.1), TaARE1-B (TraesCS7B02G196800, KAF7101772.1), TaARE1-D (TraesCS7D02G283700, KAF7108895.1); HvARE1 (HORVU7 Hv1G063720, AK375792), OsARE1 (Os08g0224300, BAT04386), GmARE1 (SORBI_3001G536901, XM_021451333.1), ZmARE1 (Zm00001d048524, NM_001139043.2), and AtARE1 (AT4G31040, AEE85850). Sequences of the ARE1 proteins were aligned with Clustal W, and then submitted to MEGAX to construct the phylogenetic trees based on the maximum-likelihood method. The number of bootstrap replications was 100. (**C**) Subcellular localization of TaARE1. Analysis of subcellular localization of TaARE1-A-YFP (yellow fluorescent protein) protein in wheat protoplasts (scale bars = 10 μm). (**D**) The relative expression levels of *TaARE1*. Analysis of the *TaARE1* expression in various tissues at the grain-filling stage by qRT-PCR. Data presented are mean values of three technical replicates with SD ($n = 3$). The data were compared to that of *TaARE1-B* using the two-tailed Student's *t*-test; *significant at $P < 0.05$, **significant at $P < 0.01$.

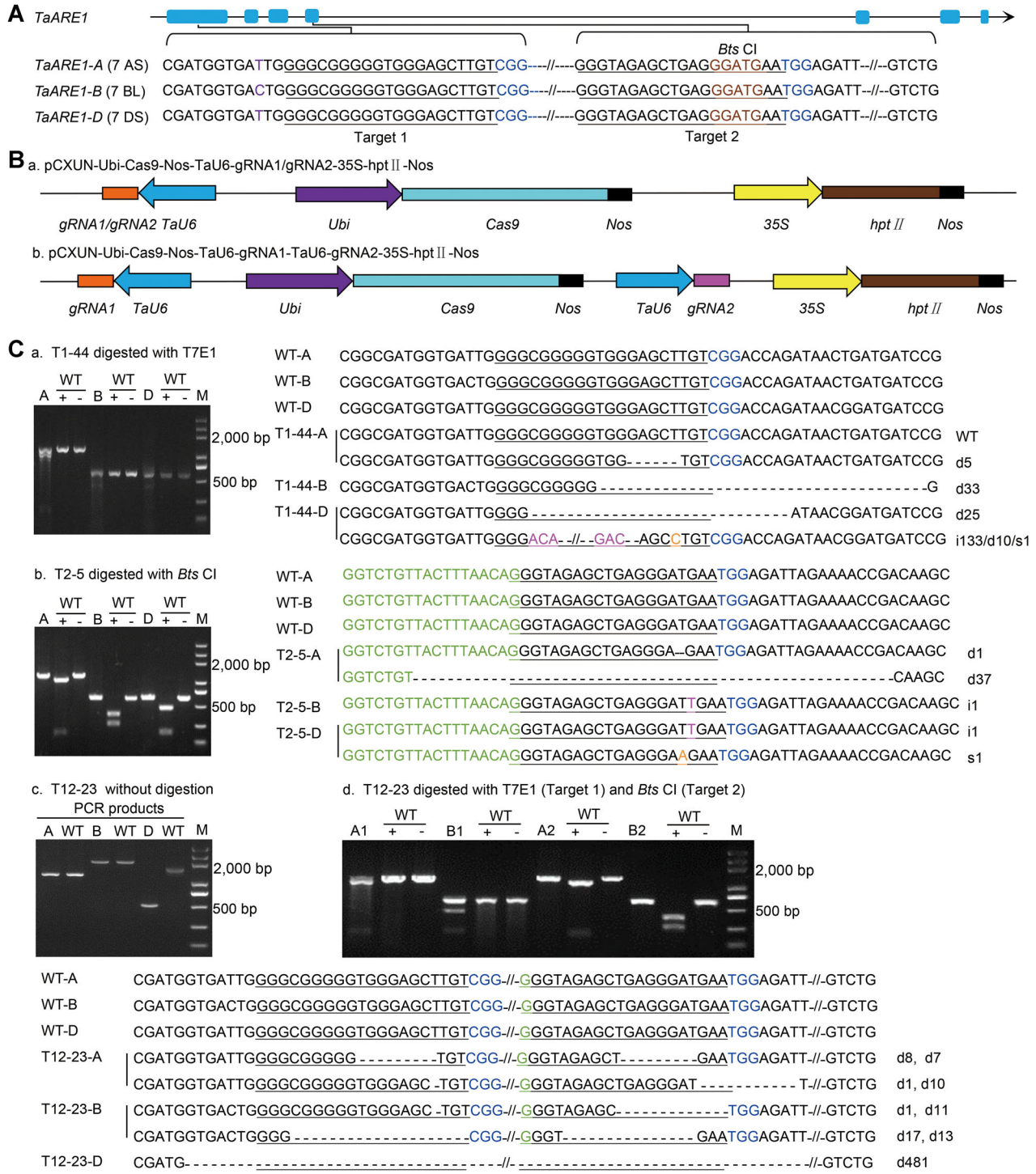

Figure 2. Continued

embryos of ZM via particle bombardment. The regenerated wheat plants were recovered after two rounds of hygromycin selection and one round of regeneration. We identified one edited plant from eleven transgenic plants for gRNA1, one edited plant from nine transgenic plants for gRNA2, and one edited plant from eight transgenic plants for gRNA1 and gRNA2 (Figure 2C). The genome-specific primers are listed in Table S1.

To investigate the off-target effects in these mutant lines, we identified 2–3 predicted potential off-target sites of these two gRNAs based on the WheatCrispr (https://crispr.bioinfo.nrc.ca/WheatCrispr/). We then used

Table 1. Transmission and segregation of CRISPR/Cas9-mediated target mutagenesis at multiple loci and transgenes from T_0 to T_1 generation

Analysis of T_0 plants				Mutation segregation in T_1 population					
Line ID	Target sites	Genotype	Induced mutations (bp)	No. of T_1 plants detected	Genotype (Ho1: He:Ho2)	Expected segregation ratio (Ho1:He:Ho2)	χ^2	*P*	*Cas9, hptII, gRNA*
T1-44	*gRNA1*	Aa	wt; d5	34	4:25:5	1:2:1	7.588	0.023	28 + : 6-
		BB	d33		34	1:2:1	0	1**	
		dd	d25; i133/ d10/s1		7:24:3	1:2:1	6.706	0.036	
T2-5	*gRNA1*	aa	d1; d37	20	5:11:4	1:2:1	7.533	0.861**	14 + : 6-
		bb	i1		20	1:2:1	0	1**	
		Dd	i1; s1		4:12:4	1:2:1	0.8	0.670**	
T12-23	*gRNA1*	aa	d8; d1	15	1:12:2	1:2:1	5.533	0.063	12 + : 3-
		bb	d1; d17		2:11:2	1:2:1	3.267	0.195*	
	gRNA2	aa	d7; d10		1:12:2	1:2:1	5.533	0.063	
		bb	d11; d13		2:11:2	1:2:1	3.267	0.195*	
	gRNA12	dd	d481		15	1:2:1	0	1**	

Notes: The capital letters A, B, and D and the lower case letters a, b, and d represent the wild-type and mutated alleles of a specific target gene in the A, B, and D subgenomes, respectively. A slash indicates that both knockout and insertion occur at the same allele and after the semicolon is the genotype of another allele. wt, wild-type; "d" indicates deletion of the indicated number of nucleotides, "i" indicates insertion of indicated number of nucleotides, "s" indicates substitution of indicated number of nucleotides. Ho1, homozygote; He, heterozygote; Ho2, homozygote. χ^2 results are shown for the closest Mendelian ratios to be observed. For transgene analysis, "+" represents that *Cas9/hptII/gRNA* are detected, and "–" shows *Cas9/hptII/gRNA* are not detected.
*$0.1 < P < 0.5$, in good agreement with 1:2:1, **$P > 0.5$, in very good agreement with 1:2:1.

genome-specific PCR combined with Sanger sequencing to detect the potential off-target mutations. No mutations were detected at the tested putative off-target sites in these mutant lines (Table S2).

Inheritance and stability of mutations, and generation of transgene-free wheat *taare1* mutant lines

We used genome-specific primers (Table S1) to genotype individual T_1 progeny to further investigate whether the CRISPR/Cas9 generated mutations could be transmitted to the next generation. We randomly selected 15–34 T_1 progenies derived from each T_0 plant for further genotyping analysis (Table 1). All of the detected mutations in the T_0 generation were transmitted to the T_1 progeny without generating new mutations. The homozygous mutation transmission rates were 100%, and heterozygous mutations were inherited according to the Mendelian ratios (homozygous/heterozygous/wild-type = 1:2:1) in the T_1 generation derived from line T2-5 (Table 1). However, the segregation patterns of lines T1-44 and T12-23 did not fit a Mendelian ratio, probably because of aberrant gamete or seed formation (Table 1).

Figure 2. CRISPR/Cas9 induced targeted mutagenesis of *TaARE1* gene in wheat
(**A**) The gene structure of *TaARE1*. Exon regions are shown as blue boxes. The SNPs among *TaARE1* homoeologs are highlighted in purple. The detail underneath shows partial sequences of *TaARE1* and its homoeologs. The sequences of target 1 (locating on exon 1 of *TaARE1*) and target 2 (locating on exon 4 of *TaARE1*) are underlined, respectively. PAM sites (5′-NGG-3′) are highlighted in blue. *Bts* CI restriction enzyme site is highlighted in brown. (**B**) Schematic presentation of the linearized CRISPR/Cas9 vectors. (a) The linearized CRISPR/Cas9 vector of gRNA1/gRNA2. (b) The linearized CRISPR/Cas9 vector of gRNA1 and gRNA2. (**C**) Detection of mutations in *TaARE1*-gRNA1 and *TaARE1*-gRNA2 via PCR/RE assay in T_0 generation. "WT", wild-type; "+", with digestion; "–", without digestion. (a) Detection of mutations in line T1-44 via PCR/T7EI assay. The PCR products of TaARE1-gRNA1 mutant lines can be digested with T7 Endonuclease I (T7EI). Line T1-44 had mutations around target 1. It contained heterozygous mutation in A genome (WT; a deletion of 5 bp), homozygous mutation in B genome (a deletion of 33 bp), and biallelic mutations in D genome (a deletion of 25 bp; an insertion of 133 bp followed by a deletion of 10 bp and a substitution of 1 bp). (b) Detection of mutations in line T2-5 via PCR/RE assay. The PCR products of TaARE1-gRNA2 mutant lines are resistant to *Bts* CI. Line T2-5 had mutations around target 2. It contained biallelic mutations in A genome (a deletion of 1 bp; a deletion of 37 bp), homozygous mutation in B genome (an insertion of 1 bp), and biallelic mutations in D (an insertion of 1 bp, a substitution of 1 bp (T-A, Asp-Glu)). (c) Detection of large fragment deletions in line T12-23 via PCR. It contained large fragment deletion in D genome. (d) Detection of mutations in line T12-23 via PCR/RE assay. The PCR products around target 1 and target 2 in line T12-23 were digested with T7EI and *Bts* CI, respectively. Line T12-23 had mutations around target 1 and target 2. It contained biallelic mutations in A genome (a deletion of 8 bp around target 1, a deletion of 7 bp around target 2; a deletion of 1 bp around target 1, a deletion of 10 bp around target 2), biallelic mutations in B genome (a deletion of 1 bp around target 1, a deletion of 11 bp around target 2; a deletion of 17 bp around target 1, a deletion of 13 bp around target 2), and homozygous mutation in D genome (a deletion of 481 bp). The PAM motifs are highlighted in blue, target sequences are underlined, insertions are highlighted in pink, substitutions are highlighted in orange, intron sequences are highlighted in green. "M", DL2000; "WT", wild-type; "d", deletion; "i", insertion; "s", substitution.

We then used primer sets designed to specifically amplify *Cas9*, the *gRNA* cassette, and *hptII* sequences to determine whether plasmid DNA was present in these mutant lines (Figure S2; Table 1). Any lines carrying transgenes were excluded from subsequent analyses. As a result, we successfully recovered *Cas9*, *gRNA* cassette, and *hptII* transgene-free plants in the T_1 generation following segregation (Figure S2). Any alleles with small deletions or insertions that caused no frame shift in the coding region were treated as wild-type alleles. Finally, we obtained one *AABBdd* line (T1-44-7) and one *aaBBdd* line (T1-44-3) derived from the T_0 line T1-44; two *aabbdd* lines (T2-5-37 and T2-5-38), and one *aabbDD* line (T2-5-63) from the T_0 line T2-5 in the T_1 generation; and one *aabbdd* line (T12-23-49) from the T_0 line T12-23 in the T_1 generation. The *a*, *b*, and *d* in these genotypes indicate null mutations of *TaARE1* in the A, B, and D subgenomes, respectively. The genotypes of these transgene-free mutant lines are listed in Table S3. The different transgene-free mutant lines enabled us to evaluate the effects of single, double, or triple-null alleles of the three *TaARE1* homoeologs from the A, B, and D subgenomes on NUE in a sole genetic background. Due to laborious works that needed to be done next, we chose the representative transgene-free T1-44-3 (*aaBBdd*), T1-44-7 (*AABBdd*), T2-5-63 (*aabbDD*) and T12-23-49 (*aabbdd*) lines for subsequent analyses (Table S3).

Root phenotypes of the mutant lines under different N conditions

The root phenotypes of different *taare1* mutant lines and the wild-type under N deficiency (0 mM NH_4NO_3) and supply (1.5 mM NH_4NO_3) hydroponic conditions are as shown in Figure 3A, 3B, and Table S4. Upon N starvation, all mutant lines exhibited decreased total root length (TRL), total root surface area (TRSA), and total root volume (TRV) compared to the wild-type, while the *aabbdd* triple-null line exhibited a significantly increased root average diameter (RAD) (Table S4). However, the root-to-shoot ratio was increased in all mutant lines under N deficiency (0 mM NH_4NO_3) or supply conditions (0.5 mM, 1.0 mM, and 1.5 mM NH_4NO_3) compared to the wild-type (Figure 3C), indicating that these mutant lines were tolerant to N starvation. Moreover, the chlorophyll content in all mutant lines retained at a higher level than that of the wild-type under all conditions, with the highest level observed in the *aabbdd* triple-null line (Figure 3D).

To further investigate the morphology of primary roots, we observed the structure of root tips and root cross sections in the different lines after 5 d of N starvation or supply treatments. For wild-type seedlings, the diameter of the elongation zone was smaller under N deficiency (0 mM NH_4NO_3) hydroponic condition (Figure 4A). The diameters increased under low N (0.5 mM and 1.0 mM NH_4NO_3) hydroponic conditions, demonstrating that low N concentration could promote the development of roots (Figure 4B, 4C). Under the high N (1.5 mM NH_4NO_3) hydroponic condition, the root diameter showed no or minor changes, indicating that the wild-type seedlings were not sensitive to high levels of N. This

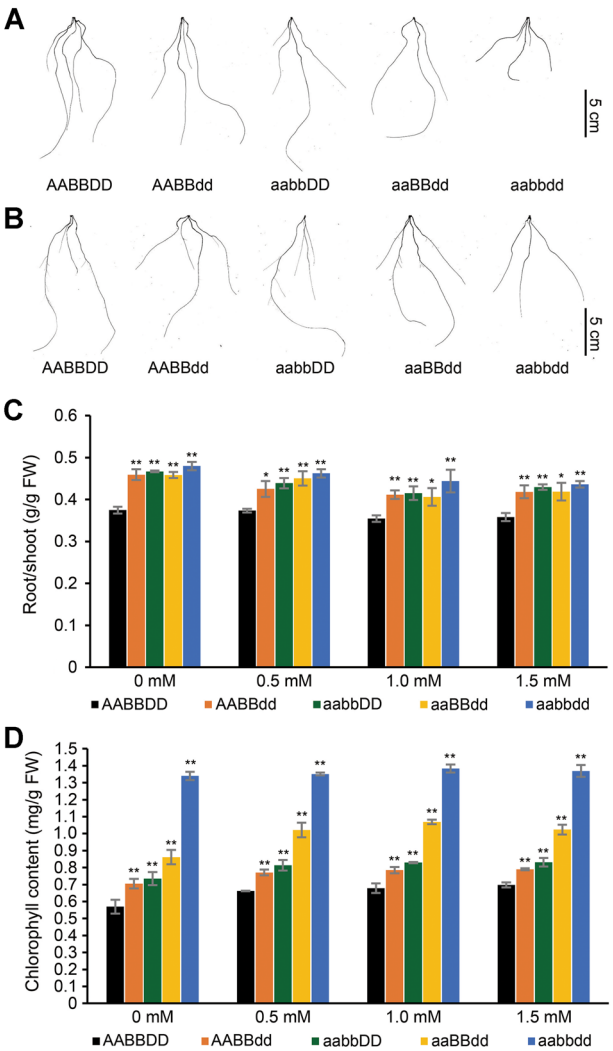

Figure 3. Root morphology, root/shoot ratio, and chlorophyll content of *taare1* mutant lines compared to the wild-type control

(A) Root morphology of wild-type and different *taare1* mutant lines under N deficiency (0 mM NH_4NO_3) hydroponic condition (scale bars = 5 cm). (B) Root morphology of wild-type and different *taare1* mutant lines under N supply (1.5 mM NH_4NO_3) hydroponic condition (scale bars = 5 cm). (C) Root/shoot ratio of wild-type and different *taare1* mutant lines under different concentrations of N (0 mM NH_4NO_3, 0.5 mM NH_4NO_3, 1.0 mM NH_4NO_3, and 1.5 mM NH_4NO_3) hydroponic conditions. (D) Quantification of chlorophyll content in wild-type and different *taare1* mutant lines under different concentrations of N (0 mM NH_4NO_3, 0.5 mM NH_4NO_3, 1.0 mM NH_4NO_3, and 1.5 mM NH_4NO_3) hydroponic conditions. For (C) and (D), data presented are mean values with SD ($n = 3$). The data were compared to that of AABBDD using the two-tailed Student's *t*-test; *significant at $P < 0.05$, **significant at $P < 0.01$.

phenomenon is consistent with a previous report showing that most modern wheat varieties cultivated after green revolution are insensitive to high N applications (Li et al., 2018). Under N starvation, the diameter of the elongation zone in the roots of the mutant lines was much larger than that of the wild-type (Figure 4A). Combined with the relative chlorophyll content in all mutant lines (Figure 3D), these results indicated that the mutant lines were tolerant to N starvation.

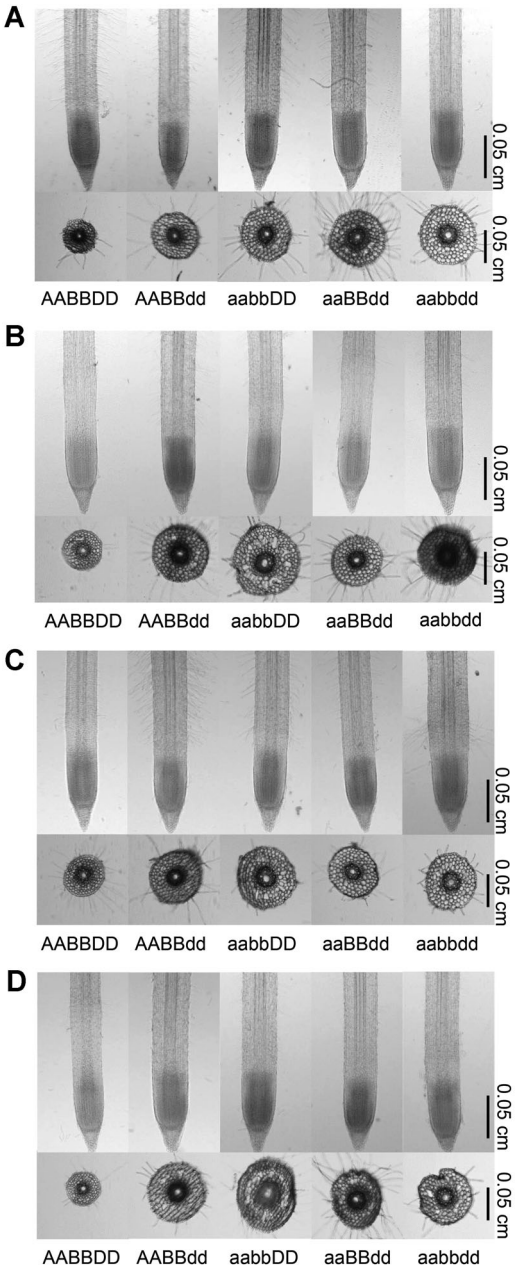

Figure 4. Morphologies of root tips and root cross sections of wild-type and different *taare1* mutant lines

The primary root tip (1.0 cm) was taken from each individual root of 5-d-old seedling, using a razor blade. Root cross sections of 0.5 cm thickness (1.0-1.5 cm distant from the primary root tip) taken from each individual root were stained for 1 min with Methylene blue solution (0.1% (w/v) in distilled water). **(A)** Morphologies of root tips and root cross sections of wild-type and different *taare1* mutant lines under N deficiency (0 mM NH_4NO_3) hydroponic condition (scale bars = 0.05 cm). **(B)** Morphologies of root tips and root cross sections of wild-type and different *taare1* mutant lines under N supply (0.5 mM NH_4NO_3) hydroponic condition (Scale bars =0.05 cm). **(C)** Morphologies of root tips and root cross sections of wild-type and different *taare1* mutant lines under N supply (1.0 mM NH_4NO_3) hydroponic condition (scale bars = 0.05 cm). **(D)** Morphologies of root tips and root cross sections of wild-type and different *taare1* mutant lines under N supply (1.5 mM NH_4NO_3) hydroponic condition (scale bars = 0.05 cm).

However, the response of the different lines exhibited different response to N treatments. When the plants were supplied with N at different concentrations, the elongation zone in the roots of the *aaBBdd* and *aabbdd* lines maintained a similar morphology as when grown under N starvation (Figure 4A–D), whereas under the low N (0.5 mM NH_4NO_3) treatment, the diameter of the primary roots from the *AABBdd* and *aabbDD* lines was significantly increased compared to when grown without N (Figure 4B). We also observed significantly enlarged root cortical cells and increased cell numbers in the different mutant lines, especially in the *AABBdd* and *aabbDD* lines, as compared to the wild-type either under N starvation or supply conditions (Figure 4A-D). An increased root cortical cell diameter corresponded with reduced energy costs of root growth in adapting to various abiotic stresses (Colombi et al., 2019). These results indicated that root phenotypes, especially the size and number of cortical cells, upon exposure to N starvation may be harnessed to improve wheat performance under N-limiting conditions.

Expression patterns of key N transport and assimilation genes upon N deprivation

We next selected four genes involved in N transport and assimilation and evaluated their expression patterns in the mutant and wild-type roots upon N deprivation. *TaAMT1*;*3b* and *TaNRT2.1* are involved in ammonium transport (Li et al., 2017) and nitrate transport (Yin et al., 2007), respectively. The cytosolic glutamine synthetase *TaGS1.1* modulates N assimilation and remobilization (Wang et al., 2020). *TaNADH-GOGAT* plays important roles in ammonium assimilation during N remobilization (Lea and Miflin, 2003; Quraishi et al., 2011).

In 2-week-old seedlings that we transferred from a N-containing solution (1.5 mM NH_4NO_3) to a N-free solution, the expression of key genes involved in N transport and assimilation was rapidly induced in the roots of the wild-type and the *taare1* mutant lines (Figure 5). The different mutant lines showed different expression patterns for *TaAMT1;3b*. *TaAMT1*;*3b* expression peaked at 1 h in the wild-type and the *aabbdd* line, but its expression of was lower overall in the *aabbdd* line than in the wild-type (Figure 5A). The *aabbDD* line showed the lowest *TaAMT1;3b* expression level, with no large fluctuation observed upon N deprivation (Figure 5A). These results indicated that the mutant lines were tolerant to N deprivation.

The expression of *TaNRT2.1* was quickly induced in the wild-type and the *aabbdd* line from 0.5 h and peaked at 1 h, but the wild-type had lower expression overall compared to the *aabbdd* line (Figure 5B). The expression of *TaNRT2.1* was induced in lines *AABBdd*, *aabbDD*, and *aaBBdd* from 0.5 h and peaked at 2 h, but the *aabbDD* line having a relatively lower expression level. Interestingly, the expression of *TaAMT1*;*3b* and *TaNRT2.1* exhibited quite different

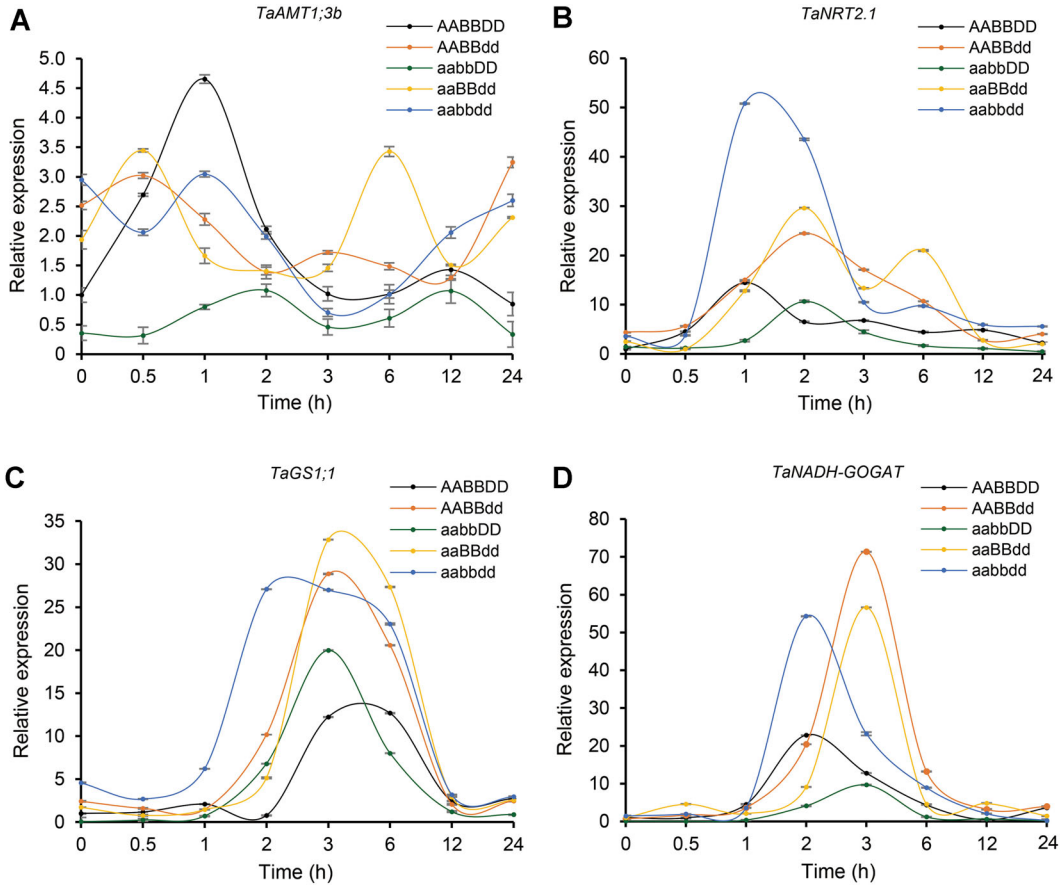

Figure 5. Expression of genes involved in N transport and assimilation in response to N deprivation

Two-week-old seedlings grown in N supply (1.5 mM NH_4NO_3) solution were transferred to N-deficiency (0 mM NH_4NO_3) solution, and then cultured for the indicated times. (A), (B) *TaAMT1;3b*, *TaNRT2.1* were key genes involved in N uptake. (C), (D) *TaGS1;1*, *TaNADH-GOGAT* were key genes involved in N assimilation. Total RNA was prepared from roots and used for qRT-PCR analysis. Data presented are mean values of 3 technical replicates with SD ($n = 3$).

profiles in the *aaBBdd* line upon N deprivation compared with other lines; for example, two expression peaks were observed (Figure 5B). These results implied that knock-out of one, two, or all three *TaARE1* homoeologs resulted in more active nitrate transport than ammonium transport upon N deprivation, and the different *TaARE1* homoeologs have diverged in this function (Figure 5A, 5B).

For *TaGS1;1* which is involved in ammonium assimilation, the relative expression levels were much higher in all mutant lines than in the wild-type (Figure 5C). The expression of *TaGS1;1* was quickly induced in the *aabbdd* triple-null line from 1 h and peaked at 2 h, whereas its expression were induced in lines *AABBdd*, *aaBBdd*, and *aabbDD* from 2 h and peaked at 3 h (Figure 5C). This result implied that knock-out of one, two, or all three *TaARE1* homoeologs resulted in more active ammonium assimilation. For *TaNADH-GOGAT* which is involved in ammonium assimilation during N remobilization, its expression was induced in the wild-type and the *aabbdd* line from 1 h and peaked at 2 h, whereas its expression in the other mutant lines peaked at 3 h (Figure 5D). In particular, the *AABBdd* line had a relatively higher *TaNADH-GOGAT* expression level among all the plants, whereas the *aabbDD* line had the lowest expression level (Figure 5D). This result implied that knock-out of *TaARE1-D* homoeologs significantly improved the assimilation of ammonium during N remobilization.

Field performances of the different mutant lines

We evaluated the field performances of the different *taare1* mutant lines and the wild-type under normal field conditions in a confined environment (Figure 6). During the early vegetative growth stages, all mutant lines showed a similar phenotype to that of the wild-type. At later growth stages, the *AABBdd* and *aabbDD* lines had a slightly increased plant height (Figures 6A, D; Table 2).

At the dough and kernel ripe stage, all the *taare1* mutant lines exhibited a stay-green phenotype and prolonged photosynthetic activity compared to the wild-type (Figure 6A–D). While the relative chlorophyll content of the wild-type and the mutant lines was maintained almost at the same level at the heading and early grain-filling stages, the relative chlorophyll content of the mutant lines was much higher than that of the wild-type at the dough stage (Table S5).

The tiller number and spike length of the *AABBdd*, *aabbDD*, and *aabbdd* lines were significantly higher than wild-type (Figures 6D, E; Table 2). However, although the largest spike length was observed in the *aabbdd* line, some

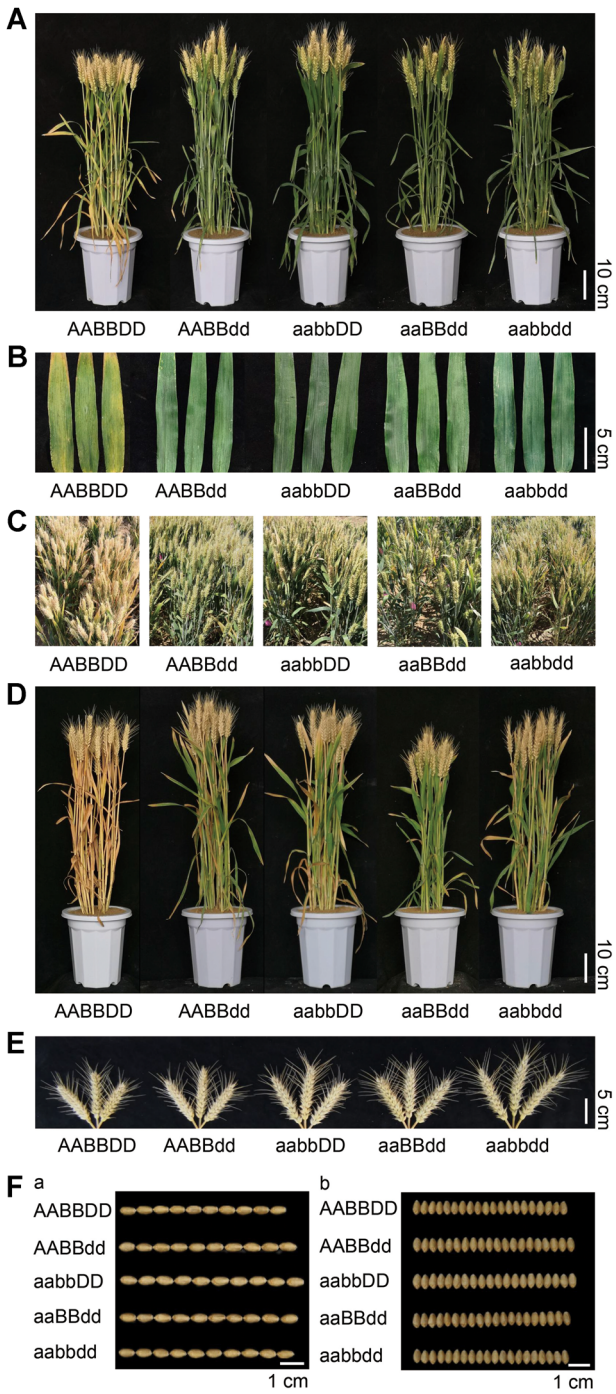

Figure 6. Phenotypes of wild-type and different *taare1* mutant lines in the field

(**A**) Plant phenotypes of wild-type and different *taare1* mutant lines at the dough stage (scale bars = 10 cm). (**B**) Phenotypes of flag leaves of wild-type and different *taare1* mutant lines at the dough stage (scale bars = 5 cm). (**C**) Plant phenotypes of wild-type and different *taare1* mutant lines at the dough stage in the field. (**D**) Plant phenotypes of wild-type and different *taare1* mutant lines at the kernel ripe stage (scale bars = 10 cm). (**E**) Spike phenotypes of wild-type and different *taare1* mutant lines at the kernel ripe stage (scale bars = 5 cm). (**F**) Grain size and appearance in wild-type and different *taare1* mutant lines at the kernel ripe stage. The grains were aligned to illustrate grain length (a) and grain width (b) between wild-type and mutant lines (scale bars = 1 cm).

of the top spikelets were infertile (Figure 6E), indicating the occurrence of growth defects when all three *TaARE1* homoeologs were knocked out. As a result, only the spikelet number and grain number per spike were higher than wild type in the *AABBdd* and *aabbDD* lines (Table 2). While the grain length of all *taare1* mutant lines was longer than that of the wild-type (Figure 6F-a; Table S5), the grain width increased significantly only in lines *AABBdd*, *aabbDD*, and *aaBBdd* (Figure 6F-b). Consequently, the 1,000-grain weight of all tested mutant lines increased in comparison with the wild-type, and in particular, the *AABBdd* and *aabbDD* lines showed significantly increased 1,000-grain weights (Table 2). Together, the field performances of the obtained mutant lines demonstrated that lines *AABBdd* and *aabbDD* could be used as novel germplasm in breeding high-yield wheat varieties.

DISCUSSION

Although wheat production has significantly increased over the past few decades, future wheat production will face unprecedented challenges in the face of increasing world population, global climate change, decreased arable land, and deteriorating environment due to intensive applications of fertilizers and pesticides. In fact, nearly all modern wheat varieties are semi-dwarf varieties with increased yield potential but reduced NUE (Li et al., 2018). Therefore, breeding of high-yield wheat varieties with improved NUE is essential for sustainable agriculture development. However, the complex genome of hexaploid wheat and gene redundancy complicate forward genetic research and wheat improvement by conventional breeding. Although various traits have been improved in wheat through genome editing (for review, please see Li et al., 2021a), improvement of both NUE and yield potential in wheat via genome editing has not been documented.

ARE1 is a negative regulator of N assimilation in rice, and its loss of function can resut in enhanced NUE and increased grain yield (Wang et al., 2018b). The *ARE1* ortholog in wheat has not been functionally characterized. In this study, we isolated and characterized three *TaARE1* homoeologs in the elite Chinese winter wheat cultivar ZM (Figure 1). We then generated a series of *taare1* transgene-free mutant lines with partial or triple-null alleles (Figure 2). All transgene-free mutant lines showed enhanced tolerance to N deficiency or deprivation under hydroponic conditions (Figures 3, 4) and showed delayed senescence and increased grain yield in a field experiment under normal growth conditions (Figure 6). The *AABBdd* and *aabbDD* mutant lines exhibited significantly enhanced NUE, delayed senescence, and increased grain yield without growth defects compared to the wild-type control (Figure 6). Thus, we generated novel wheat germplasm with improved NUE and yield potential through manipulating *TaARE1* orthologs by genome editing for the first time. Our results demonstrate the potential to manipulate

Table 2. Field performance and major yield components of wild-type and different *taare1* mutant lines

	taare1 mutant lines				
Yield components	AABBDD	AABBdd	aabbDD	aaBBdd	aabbdd
1,000-grain weight (g)	47.6 ± 0.3	54.1 ± 0.4**	56.4 ± 0.6**	53.6 ± 0.6**	53.6 ± 0.4**
Length (mm)	6.7 ± 0.1	7.1 ± 0.1**	7.3 ± 0.2**	7.1 ± 0.2**	7.0 ± 0.1**
Width (mm)	3.8 ± 0.1	4.0 ± 0.1**	4.1 ± 0.1**	3.9 ± 0.1*	3.8 ± 0.1
Plant height (cm)	68.0 ± 1.5	72 ± 1.1**	70.2 ± 1.6**	63.0 ± 2.7**	69.2 ± 1.3
Tiller number	15.7 ± 1.4	17.9 ± 2.5*	20.6 ± 1.6**	15.0 ± 2.8	19.5 ± 1.8**
Spikelet number	22.2 ± 1.6	23.8 ± 0.9*	24.4 ± 1.0**	21.0 ± 2.0	23.6 ± 2.1
Grain number of per main spike	65.4 ± 2.2	68.5 ± 3.3*	70.1 ± 3.9**	67.0 ± 6.4	68.9 ± 4.7*
Spike length (cm)	8.5 ± 0.3	9.1 ± 0.3**	9.3 ± 0.2**	8.8 ± 0.4*	10.8 ± 0.4**

*Significant at $P < 0.05$.
**Significant at $P < 0.01$.
Notes: Data presented are mean values with SD, $n = 10$; for grain length and width, $n = 20$. The data were compared to that of AABBDD using the two-tailed Student's *t*-test.

ARE1 orthologs through gene editing for breeding of high-yield wheat as well as other cereal crops with improved NUE for sustainable agricultural development.

Root system architecture (RSA) could be harnessed for increasing water and nutrient use efficiencies as well as yield potential in crop plants. The nutritional status of plants and external nutrient availability will affect root morphology. Low N stimulated primary root and lateral root elongation but not lateral root initiation. However, under severe N deprivation, lateral root formation was almost completely absent (Krouk et al., 2010; Sinha et al., 2015; Maccaferri et al., 2016). N deficiency can result in accumulation of carbohydrates in leaves and allocation of carbon to the roots, resulting in an increase in the root-to-shoot biomass ratio (Sinha et al., 2015). In this study, although all *taare1* mutant lines showed decreased TRL, TRSA, and TRV compared to the wild-type when cultured under N deficiency hydroponic condition, both the root-to-shoot ratio and the chlorophyll content were increased in all mutant lines under all conditions compared to the wild-type (Figure 3C, D). These results indicated that the mutant lines were more tolerant to N starvation and less sensitive to external N availability than the wild-type control, especially under N-limiting conditions.

Root plasticity allows the plants to optimize their root phenotypes upon exposure to abiotic stresses. High energy costs and low resource accessibility in root growth can reduce shoot growth and eventually lead to yield losses. The root cortical cell diameter was shown to be associated with the energy costs of root maintenance (Colombi et al., 2019). In this study, we observed significantly enlarged root cortical cells and increased cell numbers in the different mutant lines compared to the wild-type either under N deficiency or supply conditions (Figure 4). The increased root cortical cell size may result in decreased energy costs of root elongation to adapt to unfavorable soil condition and nutrient availability including N-limiting conditions.

To dissect the potential underlying mechanism of the differences observed among the mutant lines and the wild-type control, we examined the expression patterns of N transport and assimilation genes in the roots upon N deprivation. The expression pattern of *TaAMT1;3b* differed among the mutants, but all mutants exhibited a relatively low expression level (Figure 5A), indicating that the expression of *TaAMT1;3b* is less sensitive to N starvation than as observed in rice (Wang et al., 2018b). *TaNRT2.1* is a member of the HATS family and is a nitrate transporter that can act either as a nitrate sensor or a signal transducer to coordinate NO_3^- uptake and transport (Yin et al., 2007). When the seedlings of the mutant lines were transferred to a N-free solution, the expression level of *TaNRT2.1* was higher in the *aabbdd* line than in the wild-type control, whereas its expression differed among the *AABBdd*, *aabbDD*, and *aaBBdd* lines (Figure 5B). The results of *TaAMT1;3b* and *TaNRT2.1* expression indicated that knock-out of *TaARE1* homoeologs could stimulate nitrate transport rather than ammonium transport upon N deprivation. Furthermore, *TaARE1-D* may play an important negative role in nitrate transport since a higher level of *TaNRT2.1* expression was observed in the *AABBdd* line than in the *aabbDD* line (Figure 5B).

The relative expression level of *TaGS1;1* was much higher in all mutant lines than in the wild-type (Figure 5C), which is consistent with a previous report showing that *TaGS1.1* is the major *GS1* gene in wheat and is upregulated by low N (Wang et al., 2020). The expression of *TaNADH-GOGAT* in the wild-type and the *aabbdd* line was similar as that for *TaAMT1;3b* and *TaNRT2.1* upon N deprivation (Figure 5A, B). However, the expression of *TaNADH-GOGAT* differed among the *AABBdd*, *aabbDD*, and *aaBBdd* lines (Figure 5D), probably because these lines contain at least one functional copy of the *TaARE1* homoeologs.

Delayed leaf senescence at the grain-filling stage in crops could increase grain yield by prolonging leaf photosynthesis (Wang et al., 2018b). In this study, we observed obviously delayed senescence in different mutant lines but not in the wild-type at the dough and kernel ripe stages (Figure 6A-D; Table S5). This resulted in significantly increased spike length in *AABBdd*, *aabbDD*, and *aabbdd* lines (Figures 6D, E; Table 2). However, we noted the occurrence of growth defects when all three *TaARE1* homoeologs were knocked out (Figure 6E). Thus, only the

spikelet number and grain number per spike of lines *AABBdd* and *aabbDD* were significantly increased (Table 2). In terms of grain appearance, while the grain length of all *taare1* mutant lines was longer than those of the wild-type (Figure 6F-a), only the grain width of lines *AABBdd*, *aabbDD*, and *aaBBdd* increased significantly (Figure 6F-b). Consequently, the 1,000-grain weight of all tested mutant lines increased compared to the wild-type, in particular, the *AABBdd* and *aabbDD* lines showed significantly increased 1,000-grain weights (Table 2). The increased yield potential of the *AABBdd* and *aabbDD* lines may be attributed to the fact that *TaARE1-A* and *TaARE1-D* homoeologs had relatively higher expression levels in roots and grains than *TaARE1-B* at the grain-filling stage (Figure 1D), and that the *AABBdd* and *aabbDD* lines had significantly enlarged root cortical cells and increased cell numbers under all hydroponic conditions (Figure 4A). This suggests that at least one functional copy of either *TaARE1-A* or *TaARE1-D* is necessary for this improved yield performance (Figure 6). The field performance of the obtained mutant lines demonstrated that the *AABBdd* and *aabbDD* lines could be used as novel germplasm in breeding for high-yield wheat varieties. Meanwhile, study on
CRISPR/Cas9-mediated targeted mutagenesis of *TaARE1* gene in winter wheat variety Kenong 199 (KN199) also demon-
strates that *taare1* mutants can boost NUE and grain yield (Guo et al., 2021), indicating the immense potentials of *TaARE1* gene for the crop genetic improvement.

In conclusion, we isolated and characterized three *TaARE1* homoeologs in the elite Chinese winter wheat cultivar ZM. We then obtained a series of *taare1* transgene-free mutant lines either with partial or triple-null alleles. All transgene-free mutant lines showed enhanced tolerance to N deficiency under hydroponic conditions. We observed significantly enlarged root cortical cells and increased cell numbers in the different mutant lines, especially in lines *AABBdd* and *aabbDD* under all hydroponic conditions. Upon N deprivation, a set of genes involved in N transport and assimilation were induced with different expression patterns in different mutant lines and the wild-type control. The potential mechanism underlying these phenomena remain to be investigated in future. All mutant lines showed delayed senescence and increased grain yield in a field experiment under normal growth conditions. In particular, lines *AABBdd* and *aabbDD* exhibited significantly enhanced NUE, delayed senescence, and increased grain yield without growth defects when compared to the wild-type control. Thus, we here generated novel wheat germplasm with improved NUE and yield potential through manipulating *TaARE1* by genome editing for the first time. Our results demonstrate the potential to manipulate *ARE1* orthologs through genome editing for breeding of high-yield wheat as well as other cereal crops with improved NUE to improve agricultural sustainability and global food security.

MATERIALS AND METHODS

Identification of *ARE1* genes in the wheat genome databases and phylogenetic analysis

Based on blast analysis of the *ARE1* gene in rice (*LOC_Os08g12780*), the *ARE1* ortholog in wheat variety cultivar ZM was identified from the databases of the International Wheat Genome Sequencing Consortium, EnsemblPlants (http://plants.ensembl.org/), and a BAC library of an elite Chinese wheat variety AiKang 58 (AK). The full-length cDNA sequences of the three homoeologs of *TaARE1* were obtained by PCR using ZM cDNA as template with primer set cTaARE1-F/cTaARE1-R. The genomic structure of the *TaARE1* was illustrated by the Gene Structure Display Server (GSDS; http://gsds.cbi.pku.edu.cn/). The predicted ARE1 amino acid sequences of TaARE1-A (KAF7095826.1), TaARE1-B (KAF7101772.1), TaARE1-D (KAF7108895.1), HvARE1 (AK375792), OsARE1 (BAT04386), GmARE1 (XM_021451333.1), ZmARE1 (NM_001139043.2), and AtARE1 (AEE85850) were aligned by Clustal W (http://www.clustal.org), and then submitted to MEGAX constructing the phylogenetic tree using the maximum-likelihood method. The number of bootstrap replications was 100.

Subcellular localization of TaARE1 in wheat protoplast

In order to analyze the subcellular localization of TaARE1, a pC1390-TaARE1-A-YFP vector was constructed. First, the primer set YTaARE1-F/YTaARE1-R was used to obtain a 1,305-bp PCR fragment using ZM cDNA of *TaARE1-A* as a template. Then, the fragment was inserted into *Pst* I sites of pC1390-YFP vector to obtain pC1390-TaARE1-A-YFP vector. The primer sets are listed in Table S1.

The common wheat cultivar ZM was used for protoplast isolation. Wheat seedlings were grown at 25°C with a 16 h/8 h light/dark condition for 10 d. Stem tissues were collected and cut into 0.5–1.0mm strips. Then, the strips were transferred into 0.6-M mannitol for 10 min, followed by incubation in an enzyme solution for 4 h at 28°C with gentle shaking (40–60 rpm) in darkness. Protoplasts were washed with W5 solution, and collected using a 150μm mesh filter, followed by centrifugation at 150 *g* for 3 min. The collected protoplasts were re-suspended in W5 solution, followed by centrifugation at 150 *g* for 3 min. Afterwards, protoplasts were resuspended in MMG solution at a final concentration of $1–5\times10^6$ cells/mL. For wheat transformation, 5 μg plasmid DNA pC1390-YFP and pC1390-TaARE1-A-YFP were transformed into 100 μL fresh protoplasts by PEG-mediated transformation. The transformation process was stopped by gently adding 1.5 mL W5 solution. The protoplasts were centrifuged at 150 *g* for 3 min, followed by gently resuspension in W5 solution. Finally, the protoplasts were incubated at 25°C for 12–16 h, and then were visualized and scanned under a confocal laser scanning microscope (LSM700).

Reverse transcription quantitative PCR analysis of *TaARE1* homoeologs at the grain-filling stage

Total RNAs were extracted from root, peduncle, top second leaf, flag leaf, flag leaf sheath, spike, and grain at the grain-filling stage using TransZol Up (TransGen Biotech). Roots of seedlings under different treatments were also extracted using TransZol Up (TransGen Biotech, Beijing, China). The cDNA was synthesized using TransScript®First-Strand cDNA Synthesis SuperMix (Tiangen) according to the manufacturer's instructions. Quantitative real-time PCR (qRT-PCR) assay was performed using SuperReal PreMix Plus (SYBR Green) (Tiangen) in a CFX96TM Real-Time System (Bio-Rad). The wheat cell division control protein (CDC) gene was selected as an internal control for normalization. Sequences of all primers used in qRT-PCR are listed in Table S1. All qRT-PCR experiments were repeated in triplicate, and the mean value generated from the reference gene was used to calculate the relative gene expression of the respective target gene using the $2^{-\Delta\Delta CT}$ method.

Knockout vectors construction

The knockout vectors used in this study were based on the pCXUN-Ubi-Cas9-Nos-35S-hptII-Nos vector which contained a codon-optimized Cas9 driven by the maize (*Zea mays* L.) *ubiquitin* gene promoter. The backbone of pCXUN-Ubi-Cas9-Nos-35S-hptII-Nos contained a *hptII* for callus selection. The *Aar* I and *Sac* I sites in pCXUN-Cas9 were used for introducing the annealed gRNA oligos and the gRNA expression cassettes, respectively.

The two primer sets KTaARE1-F1/KTaARE1-R1 and KTaARE1-F2/KTaARE1-R2 were used to obtain gRNA1 and gRNA2 oligos by annealing PCR. The annealed gRNA1 and gRNA2 oligos were cloned into the linearized pCXUN-Cas9 with *Aar* I by using a pEASY-Uni Seamless Cloning and Assembly Kit (TransGen Biotech). Then, the vectors pCXUN-Ubi-Cas9-Nos-TaU6-gRNA1-35S-hptII-Nos and pCXUN-Ubi-Cas9-Nos-TaU6-gRNA2-35S-hptII-Nos were constructed. For the construction containing two gRNAs, the gRNA2 cassette was amplified by the primer set SacI-U6-F/SacI-U6-R using the plasmid of pCXUN-Ubi-Cas9-Nos-TaU6-gRNA2-35S-hptII-Nos as template. The gRNA2 cassette was cloned into the *Sac* I site of the linearized pCXUN-Ubi-Cas9-Nos-TaU6-gRNA1-35S-hptII-Nos using a pEASY-Uni Seamless Cloning and Assembly Kit, and the vector pCXUN-Ubi-Cas9-Nos-TaU6-gRNA1-TaU6-gRNA2-35S-hptII-Nos was constructed. All primer sets used in this study are listed in Table S1.

Wheat transformation

The immature wheat embryos were selected for wheat transformation. Three constructs were introduced into the immature embryos of ZM via biolistic transformation, respectively, following the previous protocol (Altpeter et al., 1996). Afterwards, the embryos were put on resting medium for 5 d and then selected on medium containing 15 mg/L and 30 mg/L hygromycin for 10 d, respectively. The vigorously grown calli were transferred to the regeneration medium (15 mg/L hygromycin) to generate green plants. Finally, the regenerated green plants were transferred to rooting medium.

Molecular characterization of different mutant lines

Genomic DNA from leaf tissue was extracted using a DNA Quick Plant System (Tiangen). PCR amplification was performed using FastPfu (TransGen Biotech) with 50 ng of genomic DNA as template. The primer set Cas9-F/Cas9-R was designed for *Cas9* detection, and the genome-specific primer set TaARE1-A-F/TaARE1-A-R was designed to amplify gRNA1 and gRNA2 of A genome; TaARE1-B1-F/TaARE1-B1-R and TaARE1-D1-F/TaARE1-D1-R were designed to amplify gRNA1; and the genome-specific primer sets TaARE1-B2-F/TaARE1-B2-R and TaARE1-D2-F/TaARE1-D2-R were designed to amplify for gRNA2. The genome-specific primer sets TaARE1-A-F/TaARE1-A-R, TaARE1-B1-F/TaARE1-B2-R, and TaARE1-D1-F/TaARE1-D2-R were designed to amplify for gRNA1 and gRNA2 to detect whether there was large fragment deletion. For the *Cas9*-positive wheat lines, the PCR products amplified for gRNA1 were digested with T7 endonuclease I (T7E1) and the PCR products amplified for gRNA2 were digested with *Bts* CI. Then, the undigested bands with *Bts* CI were recovered and directly sequenced to screen mutant plants in *TaARE1*, and the PCR products which could be digested by T7EI were also sequenced to screen *TaARE1* mutant plants. The sequence chromatograms were analyzed by a Web-based tool (http://dsdecode.scgene.com/) to check the genotype and zygosity of the tested plants (Liu et al., 2015). Some PCR products were also cloned into the pEasy-Blunt zero vector (TransGen Biotech), and at least 10 positive colonies for each sample were sequenced. The primer sets are listed in Table S1.

Off-target analysis

We selected two and three potential off-target sites to investigate the off-target effects based on the prediction of the WheatCrispr (https://crispr.bioinfo.nrc.ca/WheatCrispr/) for target 1 and target 2, individually (Table S2). Site-specific genomic PCR and Sanger sequencing were used to determine the off-target effects. The primer sets are listed in Table S1.

Hydroponic culture

Transgene-free *taare1* mutant lines in T_2 generation and wild-type were used for N treatment in hydroponic culture. For hydroponic culture, seeds were surface-sterilized with 70% ethanol for 30 s and then washed with sterile water four times. Sterilized seeds were germinated in petri dishes for 3 d, and then the seeds with residual endosperm removed were transferred to the hydroponic culture solution and fresh solution was changed every 2 d. The hydroponic culture solution contained variable concentrations of NH_4NO_3 (0 mM, 0.5 mM, 1.0 mM or 1.5 mM), 2.5 mM K_2SO_4, 1 mM KH_2PO_4, 2 mM $MgSO_4$, 0.5 mM KI, 4 mM $CaCl_2$, 0.1 mM Fe-EDTA, 0.1 mM H_3BO_3, 0.1 mM $MnSO_4$, 0.03 mM $ZnSO_4$, 1×10^{-4} mM $CuSO_4$, 0.01 mM Na_2MoO_4, and 1×10^{-4} mM $CoCl_2$, pH 6.0. Wheat seedlings were cultured in a growth

chamber under 16 h/8 h light/dark and 22°C/18°C day/night conditions. When transferring between hydroponic culture solutions containing different concentrations of NH_4NO_3, seedlings were washed in distill water 3–5 times.

RT-qPCR analysis of key genes involved in N transport and assimilation

Transgene-free *taare1* mutant lines in T_2 generation and wild-type were cultured in different hydroponic solutions as described above. After 2 weeks, seedlings in 1.5 mM NH_4NO_3 hydroponic culture solutions were transferred into N-free solution for 24 h of an N deprivation treatment. Roots of *taare1* mutant lines and wild-type were collected at 0 h, 0.5 h, 1 h, 2 h, 3 h, 6 h, 12 h, and 24 h after N-deprivation treatment. Total RNA extraction, first-strand cDNA synthesis, and qRT-PCR assay were performed as described above. Four genes, *TaAMT1*;*3b*, *TaNRT2.1, TaGS1;1*, and *TaNADH-GOGAT* involved in N transport and assimilation, were selected to evaluate the expression patterns of these genes in the roots of mutant lines and wild type upon N deprivation.

Root morphological analysis

Wheat seedlings were grown for 5 d in a nutrient solution that contained 0 mM NH_4NO_3, 0.5 mM NH_4NO_3, 1.0 mM NH_4NO_3, and 1.5 mM NH_4NO_3. The primary root tip (1.0 cm) was taken manually from each individual root using a razor blade to investigate the morphology of the elongation zone in primary roots. Root cross sections of 0.5-cm thickness (1.0–1.5 cm distant from the primary root tip) were also taken to observe the diameter of root cross sections. The cross sections were stained for 1 min with Methylene blue solution (0.1% (w/v) in distilled water) before being imaged with Zeiss Axio Imager Z2 microscope.

Roots were collected from *taare1* mutant and wild-type wheat seedlings, which were grown for 12 d in a nutrient solution containing 0 mM and 1.5 mM NH_4NO_3, individually. The root morphological parameters were analyzed with WinRHIZO software developed by Regent Instruments Canada. In terms of root and shoot ratio, dry weight of roots and shoots were measured under different hydroponic culture solutions for wild-type and *taare1* mutant wheat seedlings after 20 d.

Measurement of chlorophyll content

The total chlorophyll contents in the first leaf of 20-d-old wild-type and *taare1* mutant lines under different hydroponic culture solutions were measured according to a published protocol (Lichtenthaler, 1987). Chlorophyll was extracted with 100% ice-cold acetone and the chlorophyll content was calculated spectrophotometrically based on the absorbance of the supernatant at 644.8 nm and 661.6 nm. Samples were diluted to an optimal concentration before measuring using a spectrophotometer (Ultrospec 7000; Biochrom).

Field experiments

The field experiment was conducted at the experimental station of the Chinese Academy of Agricultural Sciences (CAAS) in Shunyi District, Beijing. The wild-type and T_2 transgene-free wheat mutant lines derived from the homozygous T_1 plants were used in the field experiment. Seeds were sown at the beginning of October, and plants were harvested in early June the next year. For each replicate of a mutant line, 45 seeds were sown in three 1.5-m-long rows, and the rows were spaced 25 cm apart. In general, 105 kg ha^{-1} of diamine phosphate and 150 kg ha^{-1} of urea were applied before sowing, and 150 kg ha^{-1} of urea was applied at the jointing stage. Other field managements were consistent with local cultivation practices of wheat varieties in the field. For each line, the 1,000-grain weight was determined according to the dry weight of 500 dried grains with at least three replicates. Grain dimensions of the matured seeds from the primary spike were measured using an electronic digital display Vernier caliper in millimeters. In addition, plant heights were recorded using a ruler in centimeters. The tiller number, spikelet number, and grain number of per main spike were recorded for 10 representative plants for each mutant line. Spike lengths were also measured using a ruler in centimeters from the base of the ear to the tip of the apical spikelet (excluding awns). The relative chlorophyll content in flag leaves of plants grown in the field was determined by a soil–plant analysis development (SPAD) value measured by a SPAD-502 Plus chlorophyll meter (Konica Minolta) following the manufacturer's instructions.

Statistical analysis

The two-tailed Student's *t*-test was used to assess the differences between the wild-type and *taare1* mutant lines. Results with a corresponding probability value of $P < 0.05$ and $P < 0.01$ were considered to be statistically significant and very significant, respectively. For each treatment, the standard deviation (SD) of the mean was calculated based on at least three biological replicates. For the χ^2 test, $P > 0.05$ was considered to be very good agreement with expected segregation ratio.

ACKNOWLEDGEMENTS

We thank Prof. Jianru Zuo for sharing unpublished data. We apologize to those whose work we were unable to cite due to space and reference limitations. This work is funded by National Key Research and Development Program of China (2020YFE0202300), the Agricultural Science and Technology Innovation Program (CAAS-ZDRW202109), Fundamental Research Funds for Central Non-Profit of Institute of Crop Sciences, Chinese Academy of Agricultural Sciences (S2021ZD03), and National Engineering Laboratory of Crop Molecular Breeding.

AUTHOR CONTRIBUTIONS

L.X. conceived and designed the experiments; J.Z., H.Z., S. L., J.L., and L.Y. performed the experiments; J.Z., H.Z., S.L., and J.L analyzed the data; L.X. and J.Z. wrote the

manuscript; and L.X. and J.L. revised the manuscript. All authors read and approved of the final manuscript.

Edited by: Zhizhong Gong, China Agricultural University, China

Received Jul. 3, 2021; **Accepted** Jul. 15, 2021; **Published** Jul. 16, 2021

OO: OnlineOpen

REFERENCES

Abe, F., Haque, E., Hisano, H., Tanaka, T., Kamiya, Y., Mikami, M., Kawaura, K., Endo, M., Onishi, K., Hayashi, T., and Sato, K. (2019). Genome-edited triple-recessive mutation alters seed dormancy in wheat. Cell Rep. **28:** 1362–1369.

Altpeter, F., Vasil, V., Srivastava, V., Stöger, E., and Vasil, I.K. (1996). Accelerated production of transgenic wheat (*Triticum aestivum* L.) plants. Plant Cell Rep. **16:** 12–17.

Biswas, S., Tian, J., Li, R., Chen, X., Luo, Z., Chen, M., Zhao, X., Zhang, D., Persson, S., Yuan, Z., and Shi, J. (2020). Investigation of CRISPR/Cas9-induced SD1 rice mutants highlights the importance of molecular characterization in plant molecular breeding. J. Genet. Genomics **47:** 273–280.

Colombi, T., Herrmann, A.M., Vallenback, P., and Keller, T. (2019). Cortical cell diameter is key to energy costs of root growth in wheat. Plant Physiol. **180:** 2049–2060.

Forde, B.G., and Lea, P.J. (2007). Glutamate in plants: Metabolism, regulation, and signalling. J. Exp. Bot. **58:** 2339–2358.

Gao, Z., Wang, Y., Chen, G., Zhang, A., Yang, S., Shang, L., Wang, D., Ruan, B., Liu, C., Jiang, H., Dong, G., Zhu, L., Hu, J., Zhang, G., Zeng, D., Guo, L., Xu, G., Teng, S., Harberd, N.P., and Qian, Q. (2019). The indica nitrate reductase gene OsNR2 allele enhances rice yield potential and nitrogen use efficiency. Nat. Commun. **10:** 1–10.

Good, A.G., and Beatty, P.H. (2011). Fertilizing nature: A tragedy of excess in the commons. PLoS Biol. **9:** e1001124.

Guo, M., Wang, Q., Zong, Y., Nian, J., Li, H., Li, J., Wang, T., Gao, C., and Zuo, J. (2021). Genetic manipulations of taare1 boost nitrogen utilization and grain yield in wheat. J. Genet. Genomics https://doi.org/10.1016/j.jgg.2021.07.003

Hu, B., Wang, W., Ou, S., Tang, J., Li, H., Che, R., Zhang, Z., Chai, X., Wang, H., Wang, Y., Liang, C., Liu, L., Piao, Z., Deng, Q., Deng, K., Xu, C., Liang, Y., Zhang, L., Li, L., and Chu, C. (2015). Variation in NRT1.1B contributes to nitrate-use divergence between rice subspecies. Nat. Genet. **47:** 834–838.

Krouk, G., Lacombe, B., Bielach, A., Perrine-Walker, F., Malinska, K., Mounier, E., Hoyerova, K., Tillard, P., Leon, S., Ljung, K., Zazimalova, E., Benkova, E., Nacry, P., and Gojon, A. (2010). Nitrate-regulated auxin transport by NRT1.1 defines a mechanism for nutrient sensing in plants. Dev. Cell **18:** 927–937.

Lea, P.J., and Miflin, B.J. (2003). Glutamate synthase and the synthesis of glutamate in plants. Plant Physiol. Biochem. **41:** 555–564.

Li, J., Luo, J., Xu, M., Li, S., Zhang, J., Li, H., Yan, L., Zhao, Y., and Xia, L. (2019). Plant genome editing using xCas9 with expanded PAM compatibility. J. Genet. Genomics **46:** 277–280.

Li, J., Jiao, G., Sun, Y., Chen, J., Zhong, Y., Yan, L., Jiang, D., Ma, Y., and Xia, L. (2021b). Modification of starch composition, structure and properties through editing of TaSBEIIa in both winter and spring wheat varieties by CRISPR/Cas9. Plant Biotechnol. J. **19:** 937–951.

Li, S., Tian, Y., Wu, K., Ye, Y., Yu, J., Zhang, J., Liu, Q., Hu, M., Li, H., Tong, Y., Harberd, N.P., and Fu, X. (2018). Modulating plant growth-metabolism coordination for sustainable agriculture. Nature **560:** 595–600.

Li, S., Zhang, C., Li, J., Yan, L., Wang, N., and Xia, L. (2021a). Present and future prospects of wheat improvement through genome editing and advanced technologies. Plant Commun. 100211.

Li, T., Liao, K., Xu, X., Gao, Y., Wang, Z., Zhu, X., Jia, B., and Xuan, Y. (2017). Wheat ammonium transporter (AMT) gene family: Diversity and possible role in host-pathogen interaction with stem rust. Front. Plant Sci. **8:** 1637.

Lichtenthaler, H.K. (1987). Chlorophylls and carotenoids: pigments of photosynthetic biomembranes. Methods Enzymol. **148:** 350–382.

Liu, C., Zhong, Y., Qi, X., Chen, M., Liu, Z., Chen, C., Tian, X., Li, J., Jiao, Y., Wang, D., Wang, Y., Li, M., Xin, M., Liu, W., Jin, W., and Chen, S. (2020). Extension of the in vivo haploid induction system from diploid maize to hexaploid wheat. Plant Biotechnol. J. **18:** 316–318.

Liu, H., Wang, K., Tang, H., Gong, Q., Du, L., Pei, X., and Ye, X. (2020). CRISPR/Cas9 editing of wheat TaQ genes alters spike morphogenesis and grain threshability. J. Genet. Genomics **47:** 563–575.

Liu, W., Xie, X., Ma, X., Li, J., Chen, J., and Liu, Y.G. (2015). DSDecode: A web-based tool for decoding of sequencing chromatograms for genotyping of targeted mutations. Mol. Plant **8:** 1431–1433.

Luo, J., Li, S., Xu, J., Yan, L., Ma, Y., and Xia, L. (2021). Pyramiding favorable alleles in an elite wheat variety in one generation by CRISPR-Cas9-mediated multiplex gene editing. Mol. Plant **14:** 847–850.

Lv, J., Yu, K., Wei, J., Gui, H., Liu, C., Liang, D., Wang, Y., Zhou, H., Carlin, R., Rich, R., Lu, T., Que, Q., Wang, W.C., Zhang, X., and Kelliher, T. (2020). Generation of paternal haploids in wheat by genome editing of the centromeric histone CENH3. Nat. Biotechnol. **38:** 1397–1401.

Lv, X., Zhang, Y., Hu, L., Zhang, Y., Zhang, B., Xia, H., Du, W., Fan, S., and Kong, L. (2021). Low-nitrogen stress stimulates lateral root initiation and nitrogen assimilation in wheat: Roles of phytohormone signaling. J. Plant Growth Regul. **40:** 436–450.

Ma, X., Zhang, Q., Zhu, Q., Liu, W., Chen, Y., Qiu, R., Wang, B., Yang, Z., Li, H., Lin, Y., Xie, Y., Shen, R., Chen, S., Wang, Z., Chen, Y., Guo, J., Chen, L., Zhao, X., Dong, Z., and Liu, Y.G. (2015). A robust CRISPR/Cas9 system for convenient, high-efficiency multiplex genome editing in monocot and dicot plants. Mol. Plant **8:** 1274–1284.

Maccaferri, M., El-Feki, W., Nazemi, G., Salvi, S., Canè, M.A., Colalongo, M.C., Stefanelli, S., and Tuberosa, R. (2016). Prioritizing quantitative trait loci for root system architecture in tetraploid wheat. J. Exp. Bot. **67:** 1161–1178.

Miller, A.J., Fan, X., Orsel, M., Smith, S.J., and Wells, D.M. (2007). Nitrate transport and signalling. J. Exp. Bot. **58:** 2297–2306.

Okada, A., Arndell, T., Borisjuk, N., Sharma, N., Watson-Haigh, N.S., Tucker, E.J., Baumann, U., Langridge, P., and Whitford, R. (2019). CRISPR/Cas9-mediated knockout of Ms1 enables the rapid generation of male-sterile hexaploid wheat lines for use in hybrid seed production. Plant Biotechnol. J. **17:** 1905–1913.

Quraishi, U.M., Abrouk, M., Murat, F., Pont, C., Foucrier, S., Desmaizieres, G., Confolent, C., Rivière, N., Charmet, G., Paux, E., Murigneux, A., Guerreiro, L., Lafarge, S., Le Gouis, J., Feuillet, C., and Salse, J. (2011). Cross-genome map based dissection of a nitrogen use efficiency ortho-metaQTL in bread wheat unravels concerted cereal genome evolution. Plant J. **65:** 745–756.

Sánchez-León, S., Gil-Humanes, J., Ozuna, C.V., Giménez, M.J., Sousa, C., Voytas, D.F., and Barro, F. (2018). Low-gluten, non-transgenic wheat engineered with CRISPR/Cas9. Plant Biotechnol. J. **16:** 902–910.

Sinha, S.K., Rani, M., Bansal, N., Gayatri, Venkatesh, K., and Mandal, P.K. (2015). Nitrate starvation induced changes in root system architecture, carbon:nitrogen metabolism, and miRNA expression in nitrogen-responsive wheat genotypes. Appl. Biochem. Biotechnol. **177:** 1299–1312.

Tang, W., Ye, J., Yao, X., Zhao, P., Xuan, W., Tian, Y., Zhang, Y., Xu, S., An, H., Chen, G., Yu, J., Wu, W., Ge, Y., Liu, X., Li, J., Zhang, H., Zhao, Y., Yang, B., Jiang, X., Peng, C., Zhou, C., Terzaghi, W., Wang, C., and Wan, J. (2019). Genome-wide associated study identifies NAC42-activated nitrate transporter conferring high nitrogen use efficiency in rice. Nat. Commun. **10:** 1–11.

Temple, S.J., Vance, C.P., and Gantt, J.S. (1998). Glutamate synthase and nitrogen assimilation. Trends Plant Sci. **3:** 51–56.

Wang, Q., Nian, J., Xie, X., Yu, H., Zhang, J., Bai, J., Dong, G., Hu, J., Bai, B., Chen, L., Xie, Q., Feng, J., Yang, X., Peng, J., Chen, F., Qian, Q., Li, J., and Zuo, J. (2018b). Genetic variations in ARE1 mediate grain yield by modulating nitrogen utilization in rice. Nat. Commun. **9:** 1–10.

Wang, Q., Su, Q., Nian, J., Zhang, J., Guo, M., Dong, G., Hu, J., Wang, R., Wei, C., Li, G., Wang, W., Guo, H.S., Lin, S., Qian, W., Xie, X., Qian, Q., Chen, F., and Zuo, J. (2021). The Ghd7 transcription factor represses ARE1 expression to enhance nitrogen utilization and grain yield in rice. Mol. Plant **14:** 1012–1023.

Wang, W., Hu, B., Yuan, D., Liu, Y., Che, R., Hu, Y., Ou, S., Liu, Y., Zhang, Z., Wang, H., Li, H., Jiang, Z., Zhang, Z., Gao, X., Qiu, Y., Meng, X., Liu, Y., Bai, Y., Liang, Y., Wang, Y., Zhang, L., Li, L., Sodmergen, Jing, H., Li, J., and Chu, C. (2018a). Expression of the nitrate transporter gene OsNRT1.1A/OsNPF6.3 confers high yield and early maturation in rice. Plant Cell **30:** 638–651.

Wang, W., Pan, Q., Tian, B., He, F., Chen, Y., Bai, G., Akhunova, A., Trick, H.N., and Akhunov, E. (2019). Gene editing of the wheat homologs of TONNEAU1-recruiting motif encoding gene affects grain shape and weight in wheat. Plant J. **100:** 251–264.

Wang, W., Simmonds, J., Pan, Q., Davidson, D., He, F., Battal, A., Akhunova, A., Trick, H.N., Uauy, C., and Akhunov, E. (2018c). Gene editing and mutagenesis reveal inter-cultivar differences and additivity in the contribution of TaGW2 homoeologues to grain size and weight in wheat. Theor. Appl. Genet. **131:** 2463–2475.

Wang, Y., Cheng, X., Shan, Q., Zhang, Y., Liu, J., Gao, C., and Qiu, J.L. (2014). Simultaneous editing of three homoeoalleles in hexaploid bread wheat confers heritable resistance to powdery mildew. Nat. Biotechnol. **32:** 947–951.

Wang, Y., Teng, W., Wang, Y., Ouyang, X., and Tong, Y. (2020). The wheat cytosolic glutamine synthetase GS1.1 modulates N assimilation and spike development by characterizing CRISPR-edited mutants. bioRxiv https://doi.org/10.1101/2020.09.03.281014

Xu, G., Fan, X., and Miller, A.J. (2012). Plant nitrogen assimilation and use efficiency. Annu. Rev. Plant Biol. **63:** 153–182.

Xu, X., Wu, K., Xu, R., Yu, J., Wang, J., Zhao, Y., Wang, Y., Song, W., Wang, S., Gao, Z., Zhong, Y., Li, X., Liao, H., and Fu, X. (2019). Pyramiding of the dep1-1 and NAL1^{NJ6} alleles achieves sustainable improvements in nitrogen-use efficiency and grain yield in japonica rice breeding. J. Genet. Genomics **46:** 325–328.

Yang, X., Nian, J., Xie, Q., Feng, J., Zhang, F., Jing, H., Zhang, J., Dong, G., Liang, Y., Peng, J., Wang, G., Qian, Q., and Zuo, J. (2016). Rice ferredoxin-dependent glutamate synthase regulates nitrogen-carbon metabolomes and is genetically differentiated between *japonica* and *indica* subspecies. Mol. Plant **9:** 1520–1534.

Yin, L.-P., Li, P., Wen, B., Taylor, D., and Berry, J.O. (2007). Characterization and expression of a high-affinity nitrate system transporter gene (TaNRT2.1) from wheat roots, and its evolutionary relationship to other NTR2 genes. Plant Sci. **172:** 621–631.

Zhan, X., Lu, Y., Zhu, J.K., and Botella, J.R. (2021). Genome editing for plant research and crop improvement. J. Integr. Plant Biol. **63:** 3–33.

Zhang, S., Zhang, Y., Li, K., Yan, M., Zhang, J., Yu, M., Tang, S., Wang, L., Qu, H., Luo, L., Xuan, W., and Xu, G. (2021). Nitrogen mediates flowering time and nitrogen use efficiency via floral regulators in rice. Curr. Biol. **31:** 671–683.

Zhang, Y., Li, D., Zhang, D., Zhao, X., Cao, X., Dong, L., Liu, J., Chen, K., Zhang, H., Gao, C., and Wang, D. (2018). Analysis of the functions of TaGW2 homoeologs in wheat grain weight and protein content traits. Plant J. **94:** 857–866.

Zhang, Z., Hua, L., Gupta, A., Tricoli, D., Edwards, K.J., Yang, B., and Li, W. (2019). Development of an *Agrobacterium*-delivered CRISPR/Cas9 system for wheat genome editing. Plant Biotechnol. J. **17:** 1623–1635.

SUPPORTING INFORMATION

Additional Supporting Information may be found online in the supporting information tab for this article: http://onlinelibrary.wiley.com/doi/10.1111/jipb.13151/suppinfo

Figure S1. cDNA sequences alignment of three *TaARE1* homoeologs
TaARE1-A, *TaARE1-B*, and *TaARE1-D* indicated the cDNA sequences of A, B and D genome. The consensus sequences were highlighted in blue. The homology level over 50% were highlighted in yellow. The similarity of *TaARE1-A*, *TaARE1-B*, and *TaARE1-D* were 99.45%.

Figure S2. Isolation of transgene-free T_1 plants from T1-44, T2-5 and T12-23 mutant lines
(**A**) A schematic description of the location/direction of the primer sets used for the analysis for the presence of T-DNA-gRNA1 sequences in T_1 plants of T1-44 (**B**), T-DNA-gRNA2 sequences in T2-5 (**C**) and T-DNA-gRNA1-gRNA2 sequences in T12-23 mutant lines (**D**). T_0 lines containing T-DNA in their genome, self-pollination allows the removal of the T-DNA in the T1 generation plants. DNA fragments of *Cas9*, *hptII*, and *gRNAs* were not detected by PCR in genomic DNA isolated from some of the T_1 plants. The control PCR product was amplified from the endogenous *Actin* gene, indicating that the genomic DNA used have sufficient quality for PCR. "-", wild-type DNA control, "+", plasmid positive control.

Table S1. Primer sets used in this study

Table S2. Analysis of potential off-target effects

Table S3. Genotypes of different transgene-free homozygous T_1 mutant lines

Table S4. Root morphological parameters of *taare1* mutant lines compared to wild-type control

Table S5. Relative chlorophyll content of wild-type and different *taare1* mutant lines at different developmental stages